MUGO: Differentiable Combinatorial Optimization for Causal Variant Discovery in the Non-coding Genome

Anonymous Author(s)

Abstract

Deciphering how non-coding variants perturb gene regulation is central to translating GWAS loci into mechanism, yet existing prioritization methods rarely deliver cell-type-resolved molecular effects, causal variant-to-gene attribution, or principled reasoning about combinatorial interactions. We introduce MUGO (Multi-head Genomic Optimization), an in silico perturbation framework that casts variant discovery as differentiable combinatorial optimization over genomic sequence. MUGO relaxes discrete edits into a continuous probabilistic nucleotide mask and performs gradient-based optimization in input space to identify single- or multi-variant perturbations that maximize a user-specified molecular objective under a sequence-to-signal foundation model. This formulation makes genome-scale search computationally tractable while retaining direct, cell-type-specific molecular readouts and enabling precise quantification of non-additive interaction effects. Across five modalities and seven tissues using two foundation-model backbones, MUGO consistently outperforms three baselines in both optimization efficiency and effect modulation, while preserving robustness and cell-type specificity. Finally, MUGO-prioritized variants are enriched for GWAS signals across diverse tissues and a broad spectrum of complex traits, turning foundation-model predictions into scalable, cell-type-resolved hypotheses for causal variant discovery and combinatorial regulatory mechanisms. Code and documentation are available at mugo-framework.netlify.app/

CCS Concepts

• **Computing methodologies** → **Machine learning**; • **Applied computing** → **Computational biology**.

Keywords

Deep Learning, Combinatorial Optimization, Causal Variant Identification, Gradient Ascent, Discrete Signal Processing

ACM Reference Format:

Anonymous Author(s). 2026. MUGO: Differentiable Combinatorial Optimization for Causal Variant Discovery in the Non-coding Genome. In *Proceedings of Proceedings of the 32nd ACM SIGKDD Conference on Knowledge Discovery and Data Mining (KDD '26).* ACM, New York, NY, USA, 20 pages. https://doi.org/XXXXXXX.XXXXXXX

Permission to make digital or hard copies of all or part of this work for personal or classroom use is granted without fee provided that copies are not made or distributed for profit or commercial advantage and that copies bear this notice and the full citation on the first page. Copyrights for components of this work owned by others than the author(s) must be honored. Abstracting with credit is permitted. To copy otherwise, or republish, to post on servers or to redistribute to lists, requires prior specific permission and/or a fee. Request permissions from permissions@acm.org.

KDD '26, Jeju, Korea

© 2026 Copyright held by the owner/author(s). Publication rights licensed to ACM.

ACM ISBN 978-1-4503-XXXX-X/26/08
https://doi.org/XXXXXXX.XXXXXXX

1 Introduction

Deciphering how genetic variants perturb gene regulation is central to translating human genetics into biological insight, improved diagnosis, and, ultimately, targeted therapies [10, 60]. Yet despite the success of genome-wide association studies (GWAS) in mapping thousands of disease-associated loci—most of which fall in the non-coding genome [6, 39]—these signals still seldom yield clear regulatory mechanisms, due to at least three persistent challenges. First, association peaks rarely yield cell-type-specific molecular interpretation, typically failing to pinpoint the perturbed regulatory element, the affected downstream program, or the direction and magnitude of effects across the specific cell types and states that mediate disease risk [7, 41]. Second, variant-to-gene causality remains difficult to establish, because linkage disequilibrium disperses statistical support across correlated variants and obscures the true causal change and its target gene(s) [19, 27, 49]. Third, existing analyses typically consider variants in isolation, limiting combinatorial reasoning about how multiple variants jointly modulate shared regulatory circuitry [40, 54]. Overcoming these barriers will require unified frameworks that can resolve causal variants, attribute their cell-type-specific molecular consequences, and model higher-order regulatory interactions.

In response to these gaps, many computational tools have emerged to prioritize candidate variants and annotate their putative functions. Widely used predictors such as CADD and FunSeq integrate diverse genomic and regulatory features to score variant deleteriousness and highlight non-coding changes likely to perturb cis-regulatory programs [15, 30, 47], while conservation-based metrics such as GERP quantify evolutionary constraint to flag nucleotides under purifying selection [12, 52]. Resources such as KEGG provide pathway-level context for genes implicated by genetic studies [24]. In parallel, statistical fine-mapping approaches—including FINEMAP, CAVIAR, PAINTOR and SuSiE, among others—aim to narrow association signals into smaller credible sets by modeling linkage disequilibrium and, in some cases, incorporating functional priors [5, 19, 26, 27, 61]. Despite these advances, most approaches still lack cell-type-specific molecular interpretation, rarely resolve variant-to-gene causality, and cannot model combinatorial effects. Consequently, quantifying variant impact—and using it for reliable interpretation and prioritization—remains challenging [62, 63].

Recent progress in deep learning—particularly sequence-to-signal foundation models that map long genomic context to regulatory readouts—has broadened what is feasible for variant interpretation [13, 31]. Starting from early demonstrations that long-range DNA sequence can predict diverse genomic tracks (e.g., DeepSEA, Basenji, Enformer) [3, 25, 66], subsequent models have improved positional resolution and expanded the predicted modalities and cell contexts (e.g., Borzoi, Sei) [9, 35], with newer efforts moving toward unified, longer-context prediction across tissues and cell types at scale (e.g., AlphaGenome, Nucleotide Transformer, HyenaDNA,

Evo) [11, 43, 44, 50]. By reducing reliance on hand-crafted features and instead learning regulatory patterns directly from sequence, these models make variant interpretation a concrete computational query: they support systematic *in silico* perturbation studies—from allele swaps and saturation mutagenesis to multi-variant edits—to quantify cell-type-specific molecular effects [59, 65], provide a basis for resolving variant-to-gene causality by tracing how allelic changes propagate through predicted regulatory intermediates to downstream gene regulation, and enable principled searches over combinatorial variant sets that amplify, buffer, or redirect regulatory programs [56]. Collectively, this paradigm offers a practical route to linking **sequence perturbation** with **molecular consequence** in a more direct and quantitative manner, thereby addressing the three challenges outlined above.

By enabling quantitative, cell-type-aware *in silico* sequence perturbations with direct readouts in predicted genomic tracks, sequence-to-signal foundation models make feature selection a natural next step: variants, motifs, or sequence segments can be edited and their molecular consequences assessed computationally. Permutation-based feature selection is therefore appealing for variant interpretation, but genome-scale applications introduce **three practical obstacles**. First, the search space is vast—$\sim$ 20,000 genes$\times$ $\sim 10^6$ variants$\times$multiple allele permutations—placing exhaustive perturbation beyond reach; genome-wide single-variant screens are already prohibitive, and higher-order combinatorial exploration is essentially impossible. Second, regulatory architecture is intrinsically combinatorial, so single-variant perturbations often miss synergy, buffering, and higher-order interactions [46, 64]. Third, many applications require global, context-robust attributions that capture patterns conserved across loci, cell types, and conditions, rather than explanations tailored to individual examples. Gradient-based shortcuts, including saliency maps, partially address computational cost but are limited by causal faithfulness, as they largely reflect local model sensitivity and can be unstable under saturation or small perturbations [29, 51, 53, 55]. These limitations motivate new methods that scale to genome-wide search while supporting combinatorial reasoning and more causally interpretable attributions.

To address these challenges, we introduce **MUGO** (**Mu**lti-head **G**enomic **O**ptimization), a framework that recasts causal variant discovery and prioritization as a **differentiable combinatorial optimization** problem. Rather than relying on discrete enumeration, MUGO uses a soft-masking relaxation inspired by recent progress in counterfactual explanation [28, 37]. Specifically, discrete DNA sequence edits are replaced with a continuous probabilistic mask over nucleotides, which makes the search space differentiable and enables end-to-end gradient ascent directly in input space [23, 38]. Candidate perturbations can then be iteratively refined toward a specified molecular objective, such as increasing or decreasing a target regulatory signal or gene expression program. We implement this strategy by coupling MUGO to the state-of-the-art open-source Borzoi architecture [35], enabling zero-shot identification of high-impact—potentially combinatorial—variant sets in a given molecular context. This design provides **three practical advantages**: (i) direct, assay-level readouts that support cell-type-specific interpretation beyond black-box scores; (ii) an explicit perturbation-based route to separate causal from merely associated variants; and (iii) a computationally efficient alternative to brute-force combinatorial search.

Our main contributions are summarized as follows:

- We propose MUGO, an efficient *in silico* perturbation-based framework that reframes variant prioritization as a controllable optimization problem, linking sequence edits to cell-type-specific molecular consequences and combinatorial (non-additive) interaction effects—thereby enabling mechanistic, experimentally actionable hypotheses beyond the existing static scoring schemes.
- Using two sequence-to-signal foundation models, we benchmark MUGO across five modalities and seven tissues, showing consistent gains over three baselines and robustness across backbones while preserving cell-type specificity and accurately quantifying combinatorial effects.
- To demonstrate utility for disease studies, we show that MUGO highlights disease-relevant variants across diverse tissues and a broad spectrum of complex traits, enabling context-specific mechanistic interpretation beyond proximity- or association-based prioritization.

2 Relation to Prior Work

Variant impact quantification or prioritization methods broadly fall into four lines: conservation or deleteriousness scores, functional impact models, population-based molecular associations, and statistical fine-mapping. We briefly review each and highlight shared limitations in cell-type-resolved interpretation, variant-to-gene causality, and combinatorial reasoning.

Conservation- and deleteriousness-based scores offer a scalable first pass for variant prioritization. Metrics such as phyloP, phastCons, and GERP, together with integrative predictors like CADD, distill evolutionary constraint and diverse genomic features into a single severity score [12, 30, 47, 52]. While useful for genome-wide triage, they are largely agnostic to cell type and state and rarely identify the perturbed regulatory process or target gene, limiting context-specific, testable hypotheses.

Functional impact models for coding and regulatory sequence aim to move beyond generic severity scores by estimating more specific consequences. For coding variants, tools such as SIFT, PolyPhen-2, and REVEL predict protein-level disruption [1, 22, 42], while non-coding methods including GWAVA, FunSeq2, and LINSIGHT leverage regulatory annotations and motif-perturbation signals [15, 21, 48]. However, many still depend on aggregated annotations or simplified sequence assumptions, limiting sensitivity to state-dependent regulation. Moreover, even when disruption is predicted, linking a variant to the causal element and downstream target gene often remains indirect [18].

Population-based molecular associations provide empirical support by linking genetic variation to molecular phenotypes. Resources such as GTEx map eQTL and sQTL effects across tissues [57, 58], and allele-specific analyses can further support regulatory hypotheses [8]. Colocalization methods (e.g., coloc, eCAVIAR) assess whether molecular and disease associations are consistent with a shared signal [17, 20]. However, limited cell-type and developmental resolution—and the lack of disease-relevant perturbation

contexts—often weakens interpretation. Moreover, linkage disequilibrium (LD) blurs variant-level attribution, and shared signals alone do not establish a causal chain from variant to regulatory element to target gene [45].

Statistical fine-mapping refines association signals by modeling linkage disequilibrium to estimate posterior inclusion probabilities and credible sets (e.g., FINEMAP, SuSiE, CAVIAR, PAINTOR), sometimes aided by functional priors [5, 19, 26, 61]. Although it sharpens prioritization, credible sets often remain sizeable in highly correlated regions, and the resulting probabilities offer limited mechanistic insight [63]. Thus, fine-mapping narrows candidates but typically does not identify the perturbed regulatory program, affected gene, or context-dependent effects.

Perturbation-based Feature Selection and Model Interpretation With the rise of deep learning "oracles," perturbation-based methods have become a standard tool for feature attribution and interpretation. *In silico mutagenesis* (ISM) [2, 66] estimates variant effects by mutating a reference base to an alternative allele and measuring the change in predicted output. However, ISM is computationally expensive $O(L)$ forward passes for a length-L sequence) and inherently local, evaluating one variant at a time and thus missing combinatorial, context-dependent regulatory effects. Higher-order extensions quickly become intractable as the search space grows exponentially [31, 56]. To reduce the cost of explicit perturbation, gradient-based attribution methods such as Saliency Maps [53], DeepLIFT [51], and Integrated Gradients [55] backpropagate prediction signals to the input to estimate feature importance in $O(1)$ time. However, in genomics these attributions are often noisy, sensitive to baseline choices and saturation, and can suffer from "shattered gradients" in deep architectures such as Transformers [4, 16]. More fundamentally, gradients are local linear approximations and may mischaracterize the non-linear effects of discrete base substitutions. Here we retain the efficiency of gradient-based optimization while improving robustness and differentiability through soft-masking and consensus mechanisms, conceptually extending generative optimization approaches [28, 33, 37] to discrete variant prioritization.

3 Methodology

In this section, we present MUGO, a differentiable framework for causal variant discovery and objective-driven sequence perturbation. In contrast to perturbation-based strategies that rely on discrete enumeration, MUGO formulates the search as a variational inference problem, enabling efficient gradient-based optimization over high-dimensional combinatorial spaces. The method iteratively refines candidate perturbations toward a user-specified molecular objective, as summarized in Fig. 1.

3.1 Problem Formulation

3.1.1 Genomic Signal and Search Space. Let $\mathcal{S} = \{A, C, G, T\}$ denote the alphabet of nucleotides. We represent the reference genomic sequence as a one-hot encoded matrix $\mathbf{X}_{\text{ref}} \in \{0,1\}^{L\times 4}$, where L is the sequence length (e.g., 524,288 bp for Borzoi). The goal of regulatory variant discovery is to identify specific mutations that significantly alter downstream biological signals, such as gene expression or chromatin accessibility.

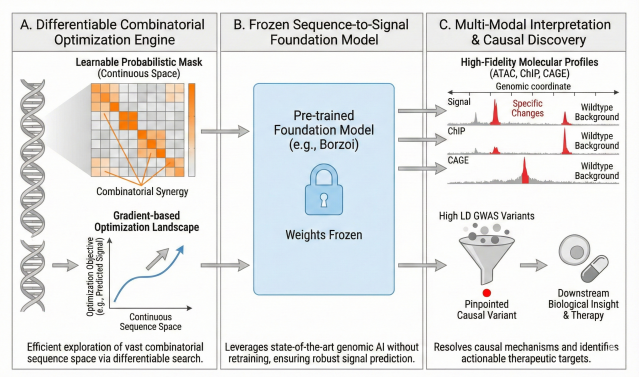

Figure 1: MUGO framework overview. (A) Engine: Gumbel-Softmax relaxation enables differentiable search over the combinatorial variant space. (B) Model: A straight-through estimator (STE) connects discrete DNA inputs to a frozen sequence-to-signal model while preserving gradient flow. (C) Discovery: Multi-modal objectives help disentangle causal variants from high-LD noise.

We constrain our optimization to a biologically valid manifold. Let $\mathcal{V} = \{v_1, v_2, \ldots, v_N\}$ be a set of candidate variants (e.g., common SNPs from the Geuvadis dataset), where each v_i is defined by a genomic position p_i and an alternative allele. This constraint is crucial to ensure that the identified variants are naturally occurring rather than synthetic adversarial perturbations.

3.1.2 Optimization Objective. Our objective is to learn a sparse binary mask $\mathbf{m} \in \{0,1\}^N$ that selects a subset of variants from $\mathcal{V}$ to maximize a target function $\mathcal{F}$. Let $\mathbf{X}_{\text{alt}}$ denote the genomic sequence where all candidate variants in $\mathcal{V}$ are applied. The optimization problem can be formally stated as finding the optimal combination mask $\mathbf{m}^*$:

$$\mathbf{m}^* = \arg\max_{\mathbf{m}\in\{0,1\}^N} \quad \mathcal{J}(\mathbf{m}) = \mathcal{F}\left(\mathbf{X}_{\text{ref}} + \mathbf{m} \odot (\mathbf{X}_{\text{alt}} - \mathbf{X}_{\text{ref}})\right) \qquad (1)$$

$$\text{s.t.} \quad \|\mathbf{m}\|_0 \le k$$

where $\mathcal{F}(\cdot)$ is a differentiable deep learning oracle (e.g., Borzoi) predicting gene expression, and k is a sparsity constraint controlling the number of selected variants. Directly solving Eq. (1) is an NP-hard combinatorial problem. The search space size is $\binom{N}{k}$, which grows exponentially with N. For a typical locus with $N = 1000$ variants, exhaustive search is computationally intractable.

3.2 Differentiable Variational Relaxation

To overcome the discreteness of the binary mask $\mathbf{m}$, we relax the problem into a continuous space using principles from **Variational Inference**. We introduce a learnable variational distribution $q_{\boldsymbol{\phi}}(\mathbf{z})$ over the selection variables $\mathbf{z}$, parameterized by real-valued logits $\boldsymbol{\phi} \in \mathbb{R}^N$.

3.2.1 Gumbel-Softmax Reparameterization. Standard categorical sampling $z \sim \text{Categorical}(\text{softmax}(\boldsymbol{\phi}))$ involves a non-differentiable arg max operation, which blocks gradient flow during backpropagation. To enable end-to-end training, we employ the **Gumbel-Softmax relaxation** [23, 38]. This technique reparameterizes the

sampling process by introducing independent Gumbel noise, allowing gradients to propagate through the stochastic samples.

Specifically, we generate a continuous relaxation vector $\mathbf{y} \in [0,1]^N$ using the following transformation:

$$\mathbf{y}_i = \frac{\exp((\phi_i + g_i)/\tau)}{\sum_{j=1}^{N} \exp((\phi_j + g_j)/\tau)} \tag{2}$$

where $g_i = -\log(-\log(u))$ with $u \sim \text{Uniform}(0,1)$.

The temperature parameter $\tau > 0$ controls the entropy of the distribution. When $\tau \to \infty$, the samples approach a uniform distribution. As $\tau \to 0$, the distribution $q_{\boldsymbol{\phi}}(\mathbf{y})$ converges to a concrete one-hot categorical distribution. In our framework, we employ an annealing schedule for τ, starting with a high temperature for exploration and gradually cooling it to encourage convergence to discrete solutions.

3.3 Bio-Plausible Gradient Estimation via STE

A unique challenge in genomic deep learning is the **Out-of-Distribution (OOD)** problem. Foundation models like Borzoi were trained strictly on discrete DNA sequences (A, C, G, T). Feeding continuous, fractional inputs (e.g., a "soft" mixture of 0.6 A + 0.4 T) during optimization can lead to undefined behavior and artifacts in the model's internal activations.

To resolve this, we strictly enforce biological discreteness during the forward pass while maintaining differentiability during the backward pass. We utilize the **Straight-Through Estimator (STE)** [?].

Forward Pass (Discretization): We discretize the soft sample $\mathbf{y}$ into a hard binary mask $\mathbf{z}_{\text{hard}}$ using a greedy argmax or thresholding operation. This ensures that the input to the oracle $\mathcal{F}$ is always a valid, discrete genomic sequence:

$$\tilde{\mathbf{X}} = \mathbf{X}_{\text{ref}} + \mathbf{z}_{\text{hard}} \odot (\mathbf{X}_{\text{alt}} - \mathbf{X}_{\text{ref}}) \tag{3}$$

Backward Pass (Gradient Flow): Since the discretization step has zero derivative almost everywhere, we approximate the gradient of the hard sample with the gradient of the soft sample. This is implemented via the stop-gradient operator $\text{sg}(\cdot)$:

$$\mathbf{z}_{\text{input}} = \mathbf{z}_{\text{hard}} - \text{sg}(\mathbf{y}) + \mathbf{y} \tag{4}$$

In this formulation, $\mathbf{z}_{\text{input}} \approx \mathbf{z}_{\text{hard}}$ numerically, but $\nabla_{\boldsymbol{\phi}} \mathbf{z}_{\text{input}} = \nabla_{\boldsymbol{\phi}} \mathbf{y}$. This trick allows the gradients from the expression loss $\nabla \mathcal{J}$ to bypass the non-differentiable discretization step and update the variational parameters $\boldsymbol{\phi}$.

3.4 Stochastic Consensus for Variance Reduction

Optimization in discrete high-dimensional spaces is prone to high variance and local optima. A single stochastic sampling trajectory might be misled by gradient noise. To mitigate this, we propose a **Multi-Head Consensus Strategy**, which can be interpreted as a Monte Carlo variance reduction technique.

We maintain an ensemble of K independent optimization heads (empirically set to $K = 10$ based on performance saturation, see Figure A1), each with its own noise trajectory. Instead of optimizing a single sample, we maximize the expected gain approximated by K Monte Carlo samples:

$$\nabla_{\boldsymbol{\phi}} \mathbb{E}_q[\mathcal{J}] \approx \frac{1}{K} \sum_{k=1}^{K} \nabla_{\boldsymbol{\phi}} \mathcal{F}_k(\mathbf{z}^{(k)}) \tag{5}$$

where $\mathbf{z}^{(k)}$ represents the variant mask sampled by the k-th head.

Mechanism. By averaging gradients across diverse heads, MUGO filters out stochastic noise (aleatoric uncertainty) inherent in the sampling process. True causal variants, which provide robust signal improvements, will receive consistent positive gradients across multiple heads, whereas spurious variants driven by random noise will have their gradients averaged out to zero. This consensus mechanism effectively acts as a "biological signal filter," stabilizing the learning process (see Proof in Appendix A5).

3.5 Optimization Algorithm and Complexity

The complete training procedure is outlined in Algorithm 1. We perform iterative gradient ascent on the variational parameters $\boldsymbol{\phi}$.

Algorithm 1 Multi-Head Genomic Optimization (MUGO)

Require: Reference Sequence $\mathbf{X}_{\text{ref}}$, Candidate Set $\mathcal{V}$, Oracle $\mathcal{F}$
Require: Hyperparams: Ensemble size K, Max steps T, Learning rate η
Initialize logits $\boldsymbol{\phi} \in \mathbb{R}^N \leftarrow \mathbf{0}$, Temp $\tau \leftarrow \tau_{max}$
Pre-compute difference tensor $\Delta\mathbf{X} = \mathbf{X}_{\text{alt}} - \mathbf{X}_{\text{ref}}$
for $t = 1$ to T **do**
  Sample noise $\mathbf{g}^{(k)} \sim \text{Gumbel}(0, I)$ for $k = 1 \dots K$
  Relaxation: $\mathbf{y}^{(k)} \leftarrow \text{Softmax}((\boldsymbol{\phi} + \mathbf{g}^{(k)})/\tau)$
  STE Discretization: $\mathbf{z}^{(k)} \leftarrow \text{Hard}(\mathbf{y}^{(k)}) - \text{sg}(\mathbf{y}^{(k)}) + \mathbf{y}^{(k)}$
  Forward Oracle: $\mathcal{L} \leftarrow -\frac{1}{K} \sum_{k=1}^{K} \mathcal{F}(\mathbf{X}_{\text{ref}} + \mathbf{z}^{(k)} \odot \Delta\mathbf{X})$
  Backward: Compute gradients $\nabla_{\boldsymbol{\phi}} \mathcal{L}$
  Update: $\boldsymbol{\phi} \leftarrow \text{Adam}(\boldsymbol{\phi}, \nabla_{\boldsymbol{\phi}} \mathcal{L}, \eta)$
  Anneal: $\tau \leftarrow \max(\tau \cdot \gamma, \tau_{min})$
end for
Return Top-k variants indices from $\boldsymbol{\phi}$

Complexity Analysis. Traditional exhaustive search requires $O(\binom{N}{k})$ inferences. In contrast, MUGO requires $O(T \times K)$ inferences, where T is the number of iterations (typically 100-200) and K is the ensemble size (e.g., 20). Since $T \times K \ll \binom{N}{k}$, our method achieves a significant speedup, enabling genome-wide application.

3.6 Evaluation Framework

Regulatory variant discovery lacks a single definitive "ground truth." To evaluate MUGO comprehensively, we adopt a multi-tiered framework spanning three key dimensions: Molecular Efficacy, Cross-Model Robustness, and Biological Causality.

3.6.1 Molecular Efficacy and Combinatorial Logic. To quantify the impact of optimized variants on molecular profiles, we define the **Predicted Gain (ΔS)** as the absolute difference in the oracle's predicted signal (e.g., summed RNA-seq coverage) between the optimized sequence $\mathbf{X}_{\text{alt}}$ and the reference $\mathbf{X}_{\text{ref}}$.

To characterize non-linear interactions (Section 4.5), we define the **Interaction Ratio (ρ)**. For a set of variants, ρ measures the ratio between the combined perturbation effect and the sum of individual marginal effects:

$$\rho = \frac{|\mathcal{F}(\mathbf{X}_{\text{comb}}) - \mathcal{F}(\mathbf{X}_{\text{ref}})|}{\sum_i |\mathcal{F}(\mathbf{X}_i) - \mathcal{F}(\mathbf{X}_{\text{ref}})|} \tag{6}$$

where $\rho \approx 1$ implies additivity, and $\rho > 1$ indicates synergistic (super-linear) logic.

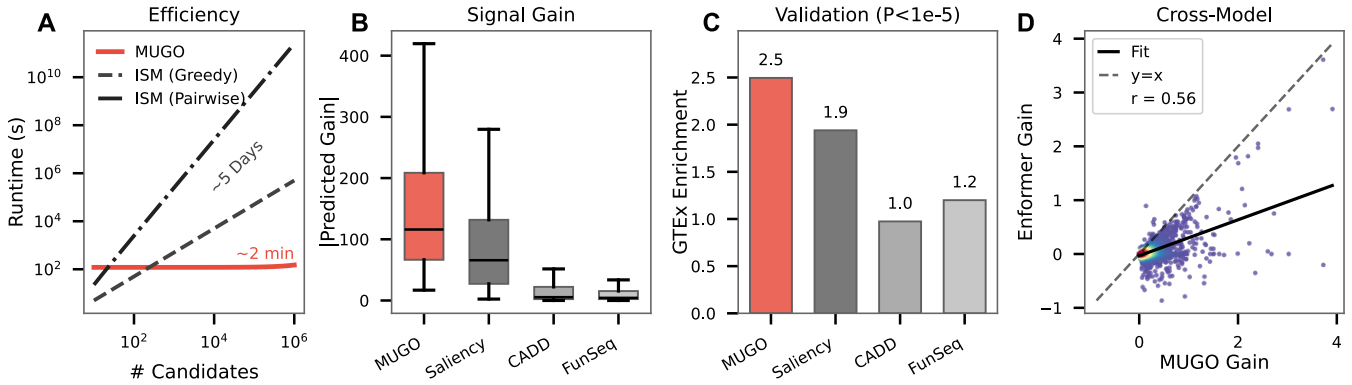

Figure 2: MUGO optimizes gene expression (summed RNA-track signal over exons) with superior efficiency and fidelity. (a) Scalability: MUGO achieves near-constant inference time, contrasting with the intractable scaling of linear (greedy) and combinatorial ISM strategies. (b) Signal Gain: MUGO consistently yields higher predicted gains compared to model-based baselines (Saliency) and non-model scoring methods (CADD, FunSeq). (c) Validation: Prioritized variants exhibit high accuracy in recovering biologically validated GTEx causal hits. (d) Robustness: Strong consistency ($r = 0.56$) between Borzoi and Enformer backbones indicates that MUGO captures intrinsic regulatory syntax rather than model-specific artifacts.

3.6.2 Independent Validation using eQTL and GWAS. We validate the biological relevance of prioritized variants using two independent reference sets: expression quantitative trait loci (eQTLs) and disease-associated GWAS variants. eQTLs provide population-level evidence that variants modulate gene expression in vivo, while GWAS variants highlight loci implicated in disease and complex traits, allowing us to test whether prioritized perturbations concentrate in genetically supported regions.

Enrichment Score. We quantify performance using the **Enrichment Score (*ES*)**, defined as the fold-increase in precision relative to random selection. Let $\hat{\mathcal{V}}_K$ be the top-K variants prioritized by the model, and $\mathcal{G}_{truth}$ be the ground-truth set (e.g., GTEx eQTLs or GWAS hits). The enrichment is calculated as:

$$ES@K = \frac{|\hat{\mathcal{V}}_K \cap \mathcal{G}_{truth}|/K}{|\mathcal{G}_{truth}|/N_{total}} \tag{7}$$

LD Resolution Stress Test. To evaluate causal discovery in high LD regions, we construct a "stress test" using fine-mapped GWAS data. For a known causal variant v_{causal} (PIP > 0.9), we identify a set of proxy variants $\mathcal{V}_{proxy}$ with high correlation ($r^2 > 0.8$). A valid interpretation method must assign a significantly higher importance score to v_{causal} than to any $v \in \mathcal{V}_{proxy}$, despite their statistical similarity.

4 Experiments

4.1 Experimental Setup

To systematically assess MUGO for decoding non-coding regulatory logic, we utilized state-of-the-art sequence-to-signal foundation models and large-scale human genetic datasets.

Datasets and Oracle Models. Our experiments focus on regulatory variation observed in human populations. We use the **Geuvadis** project [34] as the primary search space, restricting the candidate pool $\mathcal{V}$ to naturally occurring SNPs with minor allele frequency (MAF) > 0.05. For the predictive oracle, we primarily utilized **Borzoi** [36], leveraging its 524kb receptive field to capture long-range enhancer–promoter interactions. We conducted *in silico* perturbation studies across five modalities (including RNA-seq, CAGE, ATAC-seq, ChIP-seq and DNAse-seq) and seven tissues (e.g., Blood, Liver, Muscle). To ensure robustness, we replicated key results using **Enformer** [3], a Transformer-based model with distinct inductive biases (confirming that MUGO's gradient-based search generalizes effectively to Transformer architectures; see **Figure A3**).

Baselines. We benchmarked MUGO against 5 representative methods spanning four paradigms:

- **Perturbation-based:** *ISM* uses both Greedy (step-wise) and Exhaustive strategies. While considered as the "gold standard," they suffer from prohibitive scaling ($O(N)$ or $O(N^2)$).
- **Gradient-based:** *Saliency Maps* [53]. Efficient but often noisy, approximating importance via input gradients ($|\nabla_x f(x)|$).
- **Stochastic Search:** *Random Search*, serving as a baseline to quantify the necessity of gradient guidance in sparse landscapes.
- **Scoring-based:** *CADD* and *FunSeq2*. Evolutionary and annotation-based scores widely used in clinical genetics but lacking cell-type context.

Evaluation Metrics. Following the framework defined in Section 3.6, we evaluated performance using:

- **Efficiency & Efficacy:** We report Wall-clock inference time and the *Predicted Gain* (ΔS) in gene expression.
- **Robustness:** We report the Pearson correlation (r) of optimization gains between Borzoi and Enformer architectures.
- **Ground Truth Validation:** We report the *Enrichment Score (ES)* against **GTEx v8 cis-eQTLs** ($P < 10^{-5}$) for molecular relevance, and against **GWAS Catalog** variants for disease relevance.
- **Fine-Mapping Resolution:** We compare the optimization scores of fine-mapped causal variants (PIP > 0.9) versus high-LD proxies ($r^2 > 0.8$) to assess de-noising capabilities.

Table 1: Multi-modal Benchmark. Magnitude of Mean Gain ($|\overline{\Delta S}|\% \pm$ SEM). Bold indicates best performance.

Modality	Tissue	MUGO	Sal.	CADD	FunSeq
RNA-seq	Blood	**174.8** ± 18.5	58.2 ± 33.4	39.7 ± 24.3	18.8 ± 12.0
	Brain	**150.1** ± 13.3	19.8 ± 20.4	16.6 ± 11.9	2.1 ± 5.6
	Liver	**162.2** ± 15.6	48.3 ± 20.5	14.3 ± 9.6	3.6 ± 4.0
	Heart	**157.3** ± 13.7	37.1 ± 22.4	18.2 ± 12.8	4.9 ± 5.1
	Musc.	**163.7** ± 12.8	43.4 ± 24.5	19.6 ± 14.0	0.4 ± 5.1
	Lung	**108.8** ± 10.9	33.6 ± 16.2	6.0 ± 5.9	1.1 ± 4.2
	Kidney	**130.6** ± 12.6	22.9 ± 15.1	11.4 ± 9.1	6.1 ± 3.9
CAGE	Blood	**0.2** ± 0.0	0.0 ± 0.0	0.0 ± 0.0	0.0 ± 0.0
	Brain	**3.4** ± 0.3	1.2 ± 0.7	0.6 ± 0.4	0.0 ± 0.2
	Liver	**1.8** ± 0.2	0.5 ± 0.3	0.0 ± 0.1	0.0 ± 0.0
	Heart	**1.1** ± 0.1	0.4 ± 0.3	0.2 ± 0.1	0.0 ± 0.0
	Musc.	**2.3** ± 0.3	0.4 ± 0.4	0.2 ± 0.2	0.0 ± 0.1
ATAC	Blood	**0.7** ± 0.1	0.1 ± 0.1	0.0 ± 0.0	0.0 ± 0.0
	Brain	**0.8** ± 0.1	0.0 ± 0.1	0.0 ± 0.0	0.0 ± 0.0
DNAse	Blood	**5.2** ± 1.0	1.6 ± 1.0	0.2 ± 0.3	0.1 ± 0.2
	Brain	**0.8** ± 0.2	0.1 ± 0.3	0.2 ± 0.2	0.0 ± 0.0
ChIP	Blood	**26.6** ± 4.2	4.5 ± 4.9	0.5 ± 0.8	0.4 ± 1.0
	Brain	**24.5** ± 3.2	4.5 ± 4.8	0.8 ± 1.0	1.0 ± 1.2

4.2 MUGO Enables More Efficient Molecular Profile Modulation via Perturbations

We first evaluated MUGO's capacity to modulate molecular profiles along **three complementary axes**: computational efficiency, perturbation efficacy, and robustness across predictive backbones.

Computational Efficiency. Distinct from standard feature-extract methods, perturbation-based variant prioritization is fundamentally constrained by the size of the discrete search space: even under a conservative setting, it scales as $\sim 10^6$ variants $\times$ 3 candidate alleles $\times \sim$ 20,000 genes, with higher-order combinatorial searches expanding this space further. As a result, brute-force perturbation schemes such as ISM are prohibitive at scale—for example, ISM requires 5 days to prioritize a single variant for a single gene under a locus-level sweep, and an additional 500 days to identify a pair of variants that maximally modulates a target track (Fig. 1A). In contrast, MUGO replaces discrete enumeration with gradient ascent under a differentiable relaxation, enabling efficient exploration of combinatorial spaces that remain largely inaccessible to heuristic baselines. Consequently, MUGO achieves *near-constant inference time* (~2 minutes per locus, Fig. 1A) that is largely insensitive to the candidate set size, while preserving direct, model-based readouts through differentiable optimization. Furthermore, as shown in Figure A5, MUGO maintains a manageable GPU memory footprint even with large ensemble sizes ($K = 20$), fitting comfortably within 24GB consumer-grade hardware while scaling linearly in runtime.

Perturbation Efficacy. Given the prohibitive cost of brute-force perturbation, we benchmarked MUGO against representative methods from each major category of variant scoring and interpretation to assess efficacy in modulating predicted gene expression. As shown in Fig. 1B, approaches that explicitly extract actionable features for sequence editing consistently outperform non-interpretable prioritization scores in this setting. For example, MUGO and saliency-based selection achieved average gene expression changes of 174.80 and 58.20, respectively, after introducing selected mutations, exceeding model-agnostic scoring methods such as CADD and FunSeq (39.70 and 18.80; Fig. 1B). Moreover, within the feature-selection class, MUGO noticeably outperformed saliency-based baselines (174.80 vs. 58.20), highlighting the advantage of our differentiable optimization for driving targeted molecular profiles.

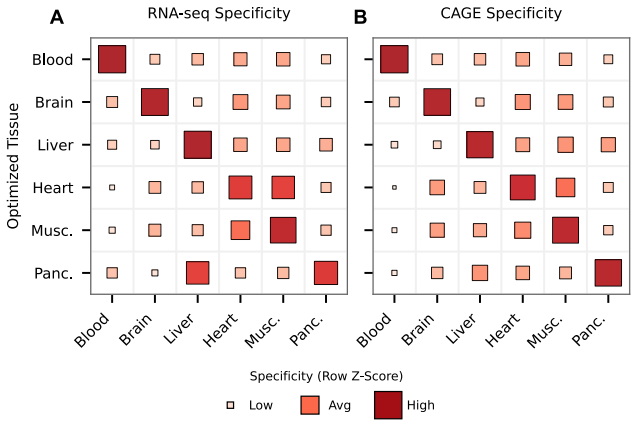

Figure 3: Multi-Modal Tissue Specificity. (a) ATAC and (b) CAGE evaluation matrices. The dominant diagonal signals confirm that MUGO-optimized variants yield maximal gains strictly within target tissues, demonstrating high cell-type specificity across chromatin and expression modalities.

Because CADD and FunSeq do not operate on a sequence-to-signal model, we performed an additional validation using independent population-based molecular evidence to assess the physiological relevance of the prioritized variants. Specifically, we curated high-confidence cis-eQTLs from the GTEx v8 resource, which nominate variants associated with gene expression in large cohorts. If a method successfully identifies variants that modulate gene expression, its prioritized set should show increased overlap with these independently supported loci. We therefore quantified the enrichment of prioritized variants relative to random selection. As shown in Fig. 1C, variants selected by MUGO achieved an enrichment of 2.50 over random, exceeding the enrichments observed for all baselines (1.94, 0.97, and 1.20 for saliency, CADD, and FunSeq, respectively). These results indicate that MUGO prioritizes variants with stronger population-level support for gene expression modulation.

Robustness across Predictive Backbones. Finally, to assess whether MUGO captures intrinsic regulatory grammar rather than model-specific artifacts of a single DNA-to-signal architecture, we performed cross-model validation. Specifically, we took variants optimized by MUGO using Borzoi and evaluated them in an independent model, Enformer, using the same loci and molecular objectives (see details in Section 3.6). We then compared the predicted gains produced by the two models to quantify cross-backbone concordance. As shown in Fig. 1D, predicted effects were strongly correlated across architectures ($r = 0.56$; detailed per-tissue comparisons are provided in Figure A2), supporting the view that the prioritized variants perturb regulatory patterns that are recognized consistently across distinct deep learning models.

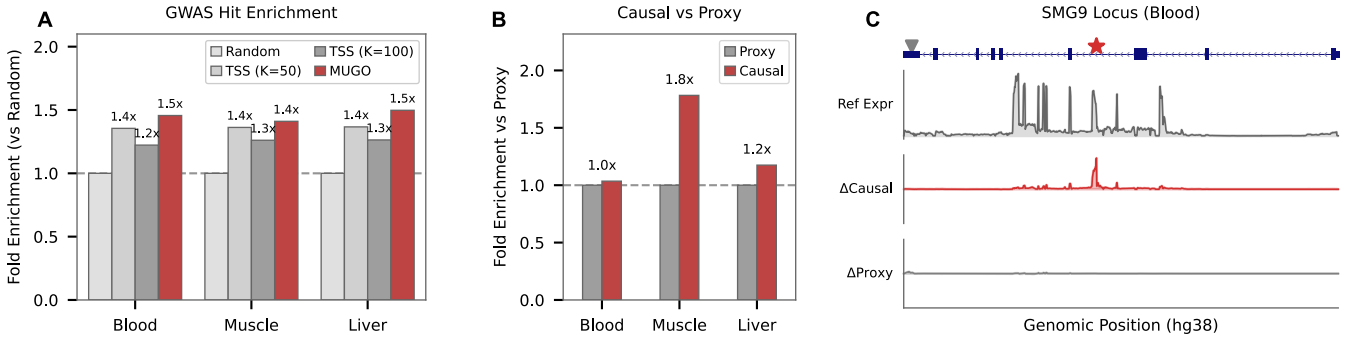

Figure 4: Resolving Variant-to-Gene Causality in High-LD Loci. (a) GWAS Enrichment: MUGO outperforms TSS-proximity and random baselines in recovering GWAS variants across tissues. (b) LD Resolution: In dense LD blocks, MUGO distinguishes causal variants (red) from correlated proxies (grey), effectively de-noising genetic signals. (c) Case Study: At the *SMG9* locus, the optimization signal (ΔCausal) selectively peaks at the causal variant, while the high-LD proxy (ΔProxy) remains silent.

4.3 MUGO Deciphers Regulatory Landscapes Across Modalities with Cell-Type Resolution

Regulatory programs are inherently multi-modal, with sequence variation propagating through coordinated changes in chromatin accessibility, histone modifications, and transcription. Moreover, these effects are often highly cell-type specific, reflecting differences in regulatory state and factor availability across cellular contexts. Motivated by these considerations, we extended our evaluation of MUGO to two additional axes: its ability to modulate molecular profiles consistently across distinct modalities, and its capacity to preserve cell-type-specific effects.

Ability for Multi-Modal Modulation We curated five modalities spanning key regulatory layers (RNA-seq, CAGE, ATAC-seq, DNAse-seq, and ChIP-seq) to evaluate MUGO in a multi-modal setting (see Section 3.6). For each modality, we assessed each method's ability to modulate targeted signal tracks across diverse tissues by introducing the corresponding sequence perturbations and measuring the resulting change in predicted signal tracks. As summarized in Table 2, model-based feature-selection approaches that leverage sequence-to-signal models consistently outperformed model-agnostic prioritization scores. In particular, MUGO and saliency-based baselines achieved average gains of 13.4- and 3.3-fold, respectively, relative to CADD and FunSeq. Notably, this improvement was not confined to a single assay or tissue (see **Figure ??**): consistent gains were observed across **all 18** of **18** test scenarios. Furthermore, MUGO outperformed saliency-based selection in **18** out of **18** tasks, supporting the advantage of differentiable combinatorial optimization for robust multi-modal modulation. Together, these results indicate that MUGO generalizes across diverse regulatory readouts and maintains strong performance across tissue contexts, providing a practical route to targeted perturbation design beyond single-modality benchmarks.

Ability to Preserve Cell-Type Specificity We next asked whether MUGO preserves cell-type specificity, which is essential for mechanistic interpretation in regulatory genomics. Using two readouts—gene expression and CAGE-derived promoter activity—we optimized variants under a tissue-specific objective and then measured their predicted effects across a panel of other tissues. As shown in Fig. 3, responses were consistently strongest in the target tissue, producing a prominent diagonal in the cross-tissue effect matrix, whereas off-diagonal signals were attenuated. These results indicate that MUGO drives tissue-targeted molecular modulation with limited cross-context leakage, consistent with context-dependent regulatory grammar rather than broadly nonspecific sequence edits.

4.4 MUGO Establishes Direct Variant-to-Gene Links for Disease-Relevant Regulatory Programs

Interpreting disease-associated variation remains a central motivation for variant prioritization, yet GWAS loci often implicate broad LD blocks and rarely pinpoint the causal mutations or their mechanistic targets. By contrast, sequence-to-signal foundation models enable direct *in silico* perturbation of candidate alleles and quantitative readouts in predicted molecular tracks, providing a more direct route from sequence edits to molecular consequences. We therefore evaluated MUGO in a disease setting by testing its ability to identify key causal mutations in different disease context.

GWAS Variants Enrichment. To evaluate the disease relevance of MUGO-prioritized variants, we measured their enrichment for tissue-matched GWAS variants relative to random expectation(Methods Section 3.6). We benchmarked against three baselines: random selection and two proximity heuristics that choose the top K variants closest to the transcription start site (TSS), with $K = 50$ and $K = 100$. Across all three tissues, MUGO consistently achieved the strongest enrichment—approximately 1.4–1.5× over random—and outperformed other strategies (Fig. 4a). This consistent pattern indicates that MUGO does not simply favor variants near genes, but preferentially recovers disease-associated signals in the appropriate tissue context, supporting its use for disease-focused variant nomination.

De-noising Variants with High LD. We tested MUGO's ability to distinguish causal variants from non-causal proxies in dense LD blocks ($r^2 > 0.8$), challenging the model to prioritize fine-mapped variants over highly correlated neighbors, which statistical association methods typically treat as nearly indistinguishable. In contrast to approaches that rely on population correlation or external annotations, MUGO scores variants using local sequence context (e.g., motif disruption). As a result, it assigns substantially higher optimization scores to causal candidates (red bars, 1.1× to 1.8×) while

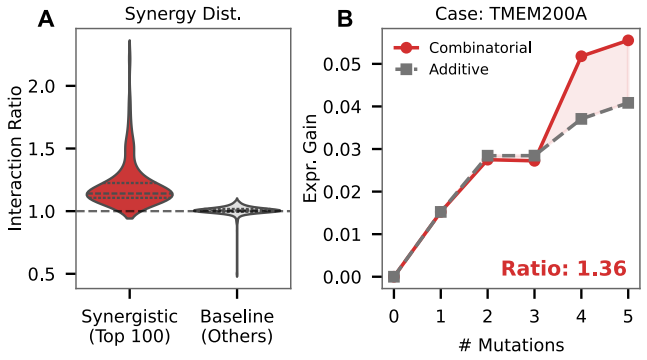

Figure 5: Uncovering Combinatorial Regulatory Logic. (a) Synergy: Top-100 synergistic genes (red) show interaction ratios > 1.0, confirming cooperative effects beyond the additive baseline. (b) Trajectory: *TMEM200A* reveals super-linear gains (red) exceeding additive expectations (grey), implying threshold-based regulation.

down-weighting high-LD proxies (grey bars, Fig. 4b)). This indicates that MUGO is sensitive to the specific disruption of regulatory grammar, rather than the variants' correlation structure.

Case Studies of Causal Variants Identified by MUGO.

We next visualized this capability using track-level predictions at the *SMG9* locus (Figure 4c). In a standard GWAS association plot, this region would appear as a broad block of correlated signals. In contrast, MUGO yields a sharp and sparse optimization peak: the predicted signal change (ΔCausal) aligns with the fine-mapped variant, whereas a statistically linked proxy produces little to no response (ΔProxy). This example highlights how deep learning–based optimization can break LD symmetry and nominate causal variants in settings where statistical genetics saturates.

4.5 MUGO Efficiently Uncovers Combinatorial Regulatory Logic

Finally, we explored non-linear variant–variant interactions within the regulatory code by probing for synergistic effects in transcriptional regulation. For example, transcription initiation often involves multiple transcription factors (TFs), and jointly perturbing these processes can produce effects that exceed the sum of individual disruptions. Such combinatorial effects are typically overlooked by existing baselines because the search space is prohibitively large. We therefore asked whether MUGO can fill in this gap to uncover this latent logic and exploit it to achieve larger optimization gains.

Identifying Synergy vs. Additivity. To quantify variant–variant interactions, we utilized the **Interaction Ratio (ρ)** (defined in Section 3.6), which normalizes the observed combinatorial gain by the sum of individual marginal gains.

Values $\rho > 1.0$ indicate positive synergy. In Figure 5a, we partitioned genes into a Synergistic tier (top-100 highest-gain genes) and a baseline tier, revealing a clear "synergy gap": the Synergistic tier is shifted above 1.0 (mean $\rho > 1.2$, with a tail > 2.0), whereas the baseline tier is tightly centered near 1.0. These results indicate that, for the most responsive genes, MUGO identifies cooperative variant clusters rather than simply aggregating independently strong variants.

To illustrate how such synergy emerges during optimization, we traced the stepwise trajectory for a representative high-synergy gene, *TMEM200A*. In Figure 5b, the grey dashed line denotes the expected additive gain (sum of individual effects), whereas the red curve shows the predicted response as variants are sequentially added.

At step 4, a specific variant triggers a super-linear spike exceeding additive expectations ($\rho = 1.36$, Fig. 5b). This suggests prioritized variants target cooperative motifs or redundant elements (e.g., shadow enhancers) [32]. Rather than functioning independently, these variants appear to engage cooperative mechanisms typically evolved to ensure phenotypic robustness and buffering against genetic perturbation; MUGO successfully identifies the specific combinatorial code required to overcome this buffering and drive a synergistic state shift.

5 Conclusion

In this work, we presented MUGO, a framework that reframes the challenge of causal variant discovery from a local attribution task to a global differentiable optimization problem. By bridging the discrete nature of genomic sequences with continuous gradient ascent via Gumbel-Softmax relaxation [23, 38] and Multi-Head Consensus, MUGO effectively navigates the combinatorial landscape of gene regulation that remains intractable for traditional perturbation baselines.

Our validation demonstrates significant advances in three key aspects. First, in terms of scalability, we achieve near-constant inference time, enabling genome-wide combinatorial screening orders of magnitude faster than *In Silico* Mutagenesis [2]. Second, regarding causality, we show that sequence-intrinsic optimization can disentangle physical drivers from statistical proxies in dense LD blocks, offering a powerful complement to population-based fine-mapping. Finally, we uncover combinatorial syntax, revealing that gene regulation is governed by non-linear synergistic interactions rather than additive effects.

While these results highlight MUGO's promise, they also point to several opportunities for further strengthening the framework. Because MUGO optimizes a model-defined molecular surrogate, the highest-scoring variants may not always translate to downstream phenotypes; integrating improved sequence-to-track-to-phenotype models and orthogonal experimental readouts should tighten this link in disease settings. In addition, increasing cell-state resolution and incorporating richer cellular context will further sharpen specificity and mechanistic interpretability. Finally, MUGO's rankings depend on the calibration and generalization of the underlying predictor, which can be challenged by distribution shifts (e.g., rare motifs or underrepresented tissue programs). Future work will therefore emphasize robustness and uncertainty quantification, enabling MUGO to report not only high-gain candidates but also well-calibrated confidence for disease-focused nomination.

As genomic foundation models continue to scale, the "signal optimization" paradigm introduced here offers a generalizable blueprint for decoding complex biological languages. Future work will extend this framework to design synthetic regulatory elements for gene therapy and explore broader multi-modal phenotypes beyond gene expression.

GenAI Disclosure

In the preparation of this work, we used Gemini to improve the readability and language quality of the manuscript. Additionally, Figure 1 was created with the assistance of Nano-banana to visually illustrate the conceptual framework. The authors reviewed and revised all AI-generated content and take full responsibility for the validity and accuracy of the final manuscript.

References

[1] Ivan A Adzhubei, Steffen Schmidt, Leonid Peshkin, Vasily E Ramensky, Anna Gerasimova, Peer Bork, Alexey S Kondrashov, and Shamil R Sunyaev. 2010. A method and server for predicting damaging missense mutations. *Nature Methods* 7, 4 (2010), 248–249.

[2] Babak Alipanahi, Andrew Delong, Matthew T. Weirauch, and Brendan J. Frey. 2015. Predicting the sequence specificities of DNA- and RNA-binding proteins by deep learning. *Nature Biotechnology* 33 (2015), 831–838.

[3] Žiga Avsec, Vikram Agarwal, Daniel Visentin, et al. 2021. Effective gene expression prediction from sequence by integrating long-range interactions. *Nature Methods* 18 (2021), 1196–1203. doi:10.1038/s41592-021-01252-x

[4] David Balduzzi et al. 2017. The Shattered Gradients Problem: If resnets are the answer, then what is the question?. In *International Conference on Machine Learning (ICML)*. 342–350.

[5] Christian Benner, Chris CA Spencer, Aki S Havulinna, Veikko Salomaa, Brian D Ripley, and Matti Pirinen. 2016. FINEMAP: efficient variable selection using summary data from genome-wide association studies. *Bioinformatics* 32, 10 (2016), 1493–1501.

[6] Annalisa Buniello, Jacqueline AL MacArthur, Maria Cerezo, Laura W Harris, James Hayhurst, Cinzia Malangone, Aoife McMahon, Joannella Morales, Edward Mountjoy, Elliot Sollis, et al. 2019. The NHGRI-EBI GWAS Catalog of published genome-wide association studies, targeted arrays and summary statistics 2019. *Nucleic Acids Research* 47, D1 (2019), D1005–D1012.

[7] Eddie Cano-Gamez and Gosia Trynka. 2020. From GWAS to function: using functional genomics to identify the mechanisms underlying complex human diseases. *Frontiers in Genetics* 11 (2020), 424.

[8] Stephane E Castel, Ami Levy-Moonshine, Pejman Mohammadi, Eric Banks, and Tuuli Lappalainen. 2015. Tools and best practices for data processing in allelic expression analysis. *Genome Biology* 16 (2015), 1–12.

[9] Kathleen M. Chen, Evan M. Cofer, Jian Zhou, et al. 2022. A sequence-based global map of regulatory activity for deciphering human genetics. *Nature Genetics* 54 (2022), 933–945. doi:10.1038/s41588-022-01102-2

[10] Melina Claussnitzer, Judy H Cho, Rory Collins, Nancy J Cox, Mark J Daly, Manuel AR Ferreira, Daniel Godt, Eric S Lander, Daniel G MacArthur, Mark I McCarthy, et al. 2020. A brief history of human disease genetics. *Nature* 577, 7789 (2020), 179–189.

[11] Hugo Dalla-Torre, Gonzalez Gonzalez, Javier Mendoza-Revilla, Nicolas L Carranza, Adam Henry Grzywaczewski, Francesco Oteri, Christian Dallago, Evan Trop, Hassan Sirelkhatim, et al. 2023. The Nucleotide Transformer: Building and Evaluating Robust Foundation Models for Human Genomics. *Bioinformatics* (2023).

[12] Eugene V Davydov, David L Goode, Marina Sirota, Gregory M Cooper, Arend Sidow, and Serafim Batzoglou. 2010. Identifying a high fraction of the human genome to be under selective constraint using GERP++. *PLoS Computational Biology* 6, 12 (2010), e1001025.

[13] Gökcen Eraslan, Žiga Avsec, Julien Gagneur, and Fabian J Theis. 2019. Deep learning: new computational modelling techniques for genomics. *Nature Reviews Genetics* 20, 7 (2019), 389–403.

[14] Adam Frankish et al. 2019. GENCODE reference annotation for the human and mouse genomes. *Nucleic Acids Research* 47, D1 (2019), D766–D773.

[15] Yao Fu, Zhiping Liu, Shaoke Lou, Jason Bedford, Xinmeng Jasmine Mu, Kevin Y Yip, Ekta Khurana, and Mark Gerstein. 2014. FunSeq2: a framework for prioritizing noncoding regulatory variants in cancer. *Genome Biology* 15, 10 (2014), 480.

[16] Amirata Ghorbani, Abubakar Abid, and James Zou. 2019. Interpretation of neural networks is fragile. *Proceedings of the AAAI Conference on Artificial Intelligence* 33, 01 (2019), 3681–3688.

[17] Claudia Giambartolomei, Damjan Vukcevic, Eric E Schadt, Lude Franke, Aroon D Hingorani, Chris Wallace, and Vincent Plagnol. 2014. Bayesian test for colocalisation between pairs of genetic association studies using summary statistics. *PLoS Genetics* 10, 5 (2014), e1004383.

[18] Albert Gu and Tri Dao. 2024. Mamba: Linear-time sequence modeling with selective state spaces. *arXiv preprint arXiv:2312.00752* (2024).

[19] Farhad Hormozdiari, Emrah Kostem, Eun Yong Kang, Bogdan Pasaniuc, and Eleazar Eskin. 2014. Identifying causal variants at loci with multiple signals of association. *Genetics* 198, 2 (2014), 497–508.

[20] Farhad Hormozdiari, Martijn Van De Bunt, Ayellet V Segrè, Xiao Li, Jong Wha J Joo, Alfred Bilow, Jae Hoon Sul, Sriram Sankararaman, Bogdan Pasaniuc, and Eleazar Eskin. 2016. Colocalization of GWAS and eQTL signals detects target genes. *American Journal of Human Genetics* 99, 6 (2016), 1245–1260.

[21] Yi-Fei Huang, Brad Gulko, and Adam Siepel. 2017. Insight into the fitness cost of human mutation from molecular evolution. *Nature Genetics* 49, 6 (2017), 905–912.

[22] Nilah M Ioannidis, Joseph H Rothstein, Vikas Pejaver, Sumit Middha, Shannon K McDonnell, Saurabh Baheti, Anthony Musolf, Qiongshi Li, Emily Holzinger, Deanna Karyadi, et al. 2016. REVEL: an ensemble method for predicting the pathogenicity of rare missense variants. *American Journal of Human Genetics* 99, 4 (2016), 877–885.

[23] Eric Jang, Shixiang Gu, and Ben Poole. 2017. Categorical Reparameterization with Gumbel-Softmax. In *International Conference on Learning Representations (ICLR)*.

[24] Minoru Kanehisa, Miho Furumichi, Mao Tanabe, Yoko Sato, and Kanae Morishima. 2017. KEGG: new perspectives on genomes, pathways, diseases and drugs. *Nucleic Acids Research* 45, D1 (2017), D353–D361.

[25] David R Kelley, Yakir A Reshef, and Maxwell Bileschi. 2018. Sequential regulatory activity prediction across chromosomes with convolutional neural networks. *Genome Research* 28, 5 (2018), 739–750.

[26] Gleb Kichaev, Megan Roytman, Ruth Johnson, Eleazar Eskin, Sara Lindstrom, Peter Kraft, and Bogdan Pasaniuc. 2017. Improved methods for multi-trait fine mapping of pleiotropic risk loci. *Bioinformatics* 33, 2 (2017), 248–255.

[27] Gleb Kichaev, Wan-Ping Yang, Sara Lindstrom, et al. 2014. Improving fine mapping of causal variants by integrating empirical candidates. *PLoS Genetics* 10, 10 (2014), e1004722.

[28] Nathan Killoran, Leo J. Lee, Andrew Delong, David K. Duvenaud, and Brendan J. Frey. 2017. Generating and designing DNA with deep generative models. In *Advances in Neural Information Processing Systems (NeurIPS)*, Vol. 30.

[29] Pieter-Jan Kindermans, Kristof Schütt, Klaus-Robert Müller, and Sven Dähne. 2016. Investigating the influence of noise and distraction on neural network optimization. *arXiv preprint arXiv:1611.04552* (2016).

[30] Martin Kircher, Daniela M Witten, Preti Jain, Brian J O'Roak, Gregory M Cooper, and Jay Shendure. 2014. A general framework for estimating the relative pathogenicity of human genetic variants. *Nature Genetics* 46, 3 (2014), 310–315.

[31] Peter K Koo and Matt Ploenzke. 2021. Representation learning of genomic sequence motifs with convolutional neural networks. *PLoS Computational Biology* 17, 7 (2021), e1009131.

[32] Evgeny Z. Kvon, Rachel Waymack, Mario Gad, and Zeba Wunderlich. 2021. Enhancer redundancy in development and disease. *Nature Reviews Genetics* 22 (2021), 324–336. doi:10.1038/s41576-020-00311-x

[33] Jack Lanchantin, Ritambhara Singh, Beilun Wang, and Yanjun Qi. 2017. Deep Motif Dashboard: Visualizing and Understanding Genomic Sequences Using Deep Neural Networks. *Pacific Symposium on Biocomputing* 22 (2017), 254–265.

[34] Tuuli Lappalainen, Michael Sammeth, Marc R Friedländer, Peter AC 't Hoen, Jean Monlong, Manuel A Rivas, Mar Gonzàlez-Porta, Scott Kuersten, Thasso Griebel, Pedro G Ferreira, et al. 2013. Transcriptome and genome sequencing uncovers functional variation in humans. *Nature* 501, 7468 (2013), 506–511.

[35] J. Linder, D. Srivastava, H. Yuan, et al. 2025. Predicting RNA-seq coverage from DNA sequence as a unifying model of gene regulation. *Nature Genetics* 57 (2025), 949–961. doi:10.1038/s41588-024-02053-6

[36] Johannes Linder, Divyansh Srivastava, Han Yuan, Vikram Agarwal, and David R Kelley. 2025. Predicting RNA-seq coverage from DNA sequence as a unifying model of gene regulation. *Nature Genetics* (2025), 1–13.

[37] Junhao Liu, Pengpeng Zhang, Martin Renqiang Min, and Jing Zhang. 2025. Identifying Combinatorial Regulatory Genes for Cell Fate Decision via Reparameterizable Subset Explanations. In *Proceedings of the 31st ACM SIGKDD Conference on Knowledge Discovery and Data Mining (KDD)*. 1823–1832. doi:10.1145/3711896.3737000

[38] Chris J. Maddison, Andriy Mnih, and Yee Whye Teh. 2017. The Concrete Distribution: A Continuous Relaxation of Discrete Random Variables. In *International Conference on Learning Representations (ICLR)*.

[39] Matthew T Maurano, Richard Humbert, Eric Rynes, Robert E Thurman, Eric Haugen, Hao Wang, Alex P Reynolds, Richard Sandstrom, Hongzhu Qu, Jennifer Brody, et al. 2012. Systematic localization of common disease-associated variation in regulatory DNA. *Science* 337, 6099 (2012), 1190–1195.

[40] Ekaterina Morgunova and Jussi Taipale. 2015. Structural insights into the cooperative binding of transcription factors to DNA. *Current Opinion in Structural Biology* 35 (2015), 1–9.

[41] Joseph Nasser, Drew T Bergman, Charles P Fulco, Philine Guckelberger, Benjamin R Doughty, Tejal A Patwardhan, Thouis R Jones, Tung H Nguyen, Jacob C Ulirsch, Fritz Lekschas, et al. 2021. Genome-wide enhancer maps link risk variants to disease genes. *Nature* 593, 7858 (2021), 238–243.

[42] Pauline C Ng and Steven Henikoff. 2003. SIFT: predicting amino acid changes that affect protein function. *Nucleic Acids Research* 31, 13 (2003), 3812–3814.

[43] Eric Nguyen, Michael Poli, Matthew Durrant, et al. 2024. Sequence modeling and design from molecular to genome scale with Evo. *Science* (2024).

[44] Eric Nguyen, Michael Poli, Marjan Faiz, Armin Thomas, et al. 2023. HyenaDNA: Long-Range Genomic Sequence Modeling at Single Nucleotide Resolution. In *Advances in Neural Information Processing Systems (NeurIPS)*, Vol. 36.

[45] Bogdan Pasaniuc and Alkes L. Price. 2017. Dissecting the genetics of complex traits using summary association statistics. *Nature Reviews Genetics* 18 (2017), 117–127.

[46] Franziska Reiter, Sebastian Wienerroither, and Alexander Stark. 2017. Combinatorial function of transcription factors and cofactors. *Current Opinion in Genetics & Development* 43 (2017), 39–46.

[47] Philipp Rentzsch, Daniela Witten, Gregory M Cooper, Jay Shendure, and Martin Kircher. 2019. CADD: predicting the deleteriousness of variants throughout the human genome. *Nucleic Acids Research* 47, D1 (2019), D886–D894.

[48] Graham RS Ritchie, Ian Dunham, Eleftheria Zeggini, and Paul Flicek. 2014. Functional annotation of noncoding sequence variants. *Nature Methods* 11, 3 (2014), 294–296.

[49] Daniel J Schaid, Wei Chen, and Nicholas B Larson. 2018. Statistical methods for identifying causal variants of complex traits. *Annual Review of Genomics and Human Genetics* 19 (2018), 391–419.

[50] Yair Schiff, Chia-Hsiang Kao, Aaron Gokaslan, et al. 2024. Caduceus: Bi-directional Equivariant Long-Range DNA Modeling. *International Conference on Machine Learning (ICML)* (2024).

[51] Avanti Shrikumar, Peyton Greenside, and Anshul Kundaje. 2017. Learning Important Features Through Propagating Activation Differences. In *Proceedings of the 34th International Conference on Machine Learning (ICML)*. 3145–3153.

[52] Adam Siepel, Gill Bejerano, Jakob S Pedersen, Angie S Hinrichs, Minmei Hou, Kate Rosenbloom, Hiram Clawson, John Spieth, LaDeana W Hillier, Stephen Richards, et al. 2005. Evolutionarily conserved elements in vertebrate, insect, worm, and yeast genomes. *Genome Research* 15, 8 (2005), 1034–1050.

[53] Karen Simonyan, Andrea Vedaldi, and Andrew Zisserman. 2013. Deep Inside Convolutional Networks: Visualising Image Classification Models and Saliency Maps. *arXiv preprint arXiv:1312.6034* (2013).

[54] François Spitz and Eileen EM Furlong. 2012. Transcription factors: from enhancer binding to developmental control. *Nature Reviews Genetics* 13, 9 (2012), 613–626.

[55] Mukund Sundararajan, Ankur Taly, and Qiqi Yan. 2017. Axiomatic Attribution for Deep Networks. In *Proceedings of the 34th International Conference on Machine Learning (ICML)*. 3319–3328.

[56] II Taskiran, K Spanier, et al. 2021. Cell-type-specific cis-regulatory elements in genetic disease constructs. *Nature Genetics* (2021).

[57] The GTEx Consortium. 2013. The Genotype-Tissue Expression (GTEx) project. *Nature Genetics* 45 (2013), 580–585.

[58] The GTEx Consortium. 2020. The GTEx Consortium atlas of genetic regulatory effects across human tissues. *Science* 369, 6509 (2020), 1318–1330.

[59] Shushan Toneyan, Ziqi Tang, and Peter K Koo. 2022. Evaluating deep learning for predicting epigenomic profiles. *Nature Machine Intelligence* 4 (2022), 766–773.

[60] Peter M Visscher, Naomi R Wray, Qian Zhang, Pamela Sklar, Mark I McCarthy, Matthew A Brown, and Jian Yang. 2017. 10 years of GWAS discovery: biology, function, and translation. *American Journal of Human Genetics* 101, 1 (2017), 5–22.

[61] Gao Wang, Abhishek Sarkar, Peter Carbonetto, and Matthew Stephens. 2020. A simple new approach to variable selection in regression, with application to genetic fine-mapping. *Journal of the Royal Statistical Society Series B: Statistical Methodology* 82, 5 (2020), 1273–1300.

[62] Christopher Weeks, Henry Lu, Chen Wang, Ruoyao Sun, Shushan Toneyan, Gökcen Eraslan, Žiga Avsec, et al. 2023. Leveraging deep learning to understand the genetics of human disease. *Nature Reviews Genetics* (2023), 1–21.

[63] Omer Weissbrod, Farhad Hormozdiari, Christian Benner, Ran Cui, Jacob Ulirsch, Steven Gazal, Armin P Schoech, Bryce Van De Geijn, Yakir Reshef, Carla Márquez-Luna, et al. 2020. Functionally informed fine-mapping and polygenic localization of complex trait heritability. *Nature Genetics* 52, 12 (2020), 1355–1363.

[64] Julia Zeitlinger. 2023. Combinatorial transcription factor binding and the problem of non-coding variant interpretation. *Current Opinion in Genetics & Development* 80 (2023), 102047.

[65] Anna Zhivi, Xiaoting Zhong, et al. 2023. Genome-wide prediction of disease variants with a deep learning framework. *Nature Communications* 14 (2023).

[66] Jian Zhou and Olga G Troyanskaya. 2015. Predicting effects of noncoding variants with deep learning-based sequence model. *Nature Methods* 12, 10 (2015), 931–934.

Appendix for: MUGO: Differentiable Combinatorial Optimization for Causal Variant Discovery

Contents

A1 Dataset and Search Space

A1.1 Genomic Sequence Data

We utilized the standard human reference genome (GRCh38). The input sequences were extracted corresponding to the specific input window requirements of our oracle models: 524,288 bp for Borzoi and 196,608 bp for Enformer. The input data $\mathbf{X}_{\text{ref}}$ is one-hot encoded into a $L \times 4$ matrix, representing the channels (A, C, G, T).

A1.2 Variant Candidate Set (Geuvadis)

To ensure biological validity, we constrained our search space $\mathcal{V}$ to naturally occurring variants. We sourced genotype data from the Geuvadis project (1000 Genomes Project Phase 3). We filtered for Single Nucleotide Polymorphisms (SNPs) with a Minor Allele Frequency (MAF) > 0.05 within the target gene regulatory windows. This filtering ensures that the optimized sequences remain on the manifold of realistic human genetic variation.

A2 Oracle Inference and Metrics

A2.1 Model Architecture and Inference

We leveraged the Borzoi architecture [35], a state-of-the-art sequence-to-profile deep learning model. Borzoi takes a genomic sequence of 524,288 base pairs (bp) as input and predicts epigenetic coverage tracks at a resolution of 32 bp per bin. To specifically target regulatory

mechanisms relevant to our validation data (Geuvadis/GTEx), we restricted the model output to tracks corresponding to **Whole Blood** tissue. We specifically selected the CAGE:Blood and RNA-seq:Blood output heads that align with the lymphoblastoid cell lines used in the validation datasets.

A2.2 Gene Expression Calculation

Unlike standard variant effect prediction tasks that rely on global signal aggregation, we implemented a precise, gene-centric quantification strategy. For each target gene, we first retrieved its canonical transcript annotation from the Gencode v41 reference [14]. We then identified the specific 32-bp output bins that spatially overlap with the gene's exons.

The predicted gene expression level y_{gene} was computed by summing the predicted coverage values solely across these exon-overlapping bins:

$$y_{gene} = \sum_{b \in \mathcal{B}_{exons}} \hat{y}_b \tag{8}$$

where $\mathcal{B}_{exons}$ represents the set of bins mapping to the exonic regions. This ensures that our optimization objective maximizes the actual transcriptional output rather than non-specific intergenic noise.

A3 Validation Strategy and Protocols

To strictly evaluate the biological causality of our optimized variants, we established a rigorous cross-dataset verification protocol. Our validation strategy consists of three key components:

- **Ground Truth Construction (GTEx Oracle):** We utilized the Genotype-Tissue Expression (GTEx) v8 project [57] as our external oracle. Specifically, we focused on Whole Blood tissue to align with the Geuvadis context. A variant is labeled as a "positive causal variant" only if it meets high-confidence criteria: a significant cis-eQTL nominal p-value ($p < 10^{-10}$) or a high Fine-mapping Posterior Probability of Inclusion (PIP > 0.1).
- **LD-Aware Evaluation Protocol:** A major challenge in genomic optimization is distinguishing causal variants from those in Linkage Disequilibrium (LD). Instead of a broad correlation scan, we specifically targeted "dense LD regions" where multiple variants are highly correlated ($r^2 > 0.8$). We evaluate whether the model can prioritize the specific SNP with the highest causal probability (Fine-mapped ID) over its correlated neighbors, effectively using high-LD non-causal variants as "Hard Negatives."
- **Quantitative Metrics:** We assess performance using two primary metrics:
  (1) **Top-k Recall:** The proportion of experimentally validated causal variants recovered within the model's top-k ranked candidates.
  (2) **Consensus Consistency:** Measuring the stability of selected variants across different initialization seeds to rule out stochastic noise.

A4 Implementation Details

A4.1 Computational Environment

All experiments were conducted on a high-performance computing cluster equipped with NVIDIA A100 (80GB) and V100 (32GB) GPUs. The framework was implemented in Python 3.9 using PyTorch 2.0. We utilized the Hugging Face Transformers library for loading pre-trained genomic models.

A4.2 Hyperparameter Settings

Table A1 lists the detailed hyperparameters used in our main experiments.

Table A1: Hyperparameter settings for MUGO optimization.

Parameter	Value
Optimizer	Adam
Learning Rate (η)	1×10^{-2}
Batch Size	1 (Sequence-specific optimization)
Max Iterations (T)	200
Initial Temperature (τ_{max})	1.0
Min Temperature (τ_{min})	0.01
Annealing Rate (γ)	1×10^{-5} (exponential decay)
Ensemble Heads (K)	20
Sparsity Constraint (k)	Top-5 variants
Gradient Clip Norm	1.0

A5 Theoretical Framework

A5.1 Problem Formulation and Objective

Our goal is to find a binary mask $\mathbf{m}$ that maximizes the expression shift. The constrained optimization problem is:

$$\max_{\mathbf{m}\in\{0,1\}^N} \mathcal{J}(\mathbf{m}) = \mathcal{F}\left(\mathbf{X}_{\text{ref}} + \mathbf{m} \odot (\mathbf{X}_{\text{alt}} - \mathbf{X}_{\text{ref}})\right) \quad \text{s.t.} \quad \|\mathbf{m}\|_0 \leq k \tag{9}$$

Direct optimization is intractable due to the 2^N search space. We relax $\mathbf{m}$ to a continuous variational distribution.

A5.2 Gumbel-Softmax Relaxation

We introduce a variational distribution $q_{\boldsymbol{\phi}}(\mathbf{z})$ parameterized by logits $\boldsymbol{\phi}$. To enable backpropagation through the sampling process, we use the Gumbel-Softmax trick. A continuous sample $\mathbf{y}$ is drawn as:

$$\mathbf{y}_i = \frac{\exp((\phi_i + g_i)/\tau)}{\sum_j \exp((\phi_j + g_j)/\tau)} \tag{10}$$

where $g_i \sim \text{Gumbel}(0, 1)$. The gradient of the loss $\mathcal{L}$ with respect to the logits ϕ_i flows via the chain rule:

$$\frac{\partial \mathcal{L}}{\partial \phi_i} = \sum_{j=1}^{N} \frac{\partial \mathcal{L}}{\partial y_j} \cdot \frac{\partial y_j}{\partial \phi_i} \tag{11}$$

This allows us to update $\boldsymbol{\phi}$ using standard gradient ascent.

A5.3 Straight-Through Estimator (STE)

To ensure valid discrete DNA inputs (A/C/G/T) while maintaining differentiability, we employ the Straight-Through Estimator. Let $\mathbf{z}_{\text{hard}} = \text{Hard}(\mathbf{y})$ be the discretized one-hot vector. The input to the model is constructed as:

$$\mathbf{z}_{\text{input}} = \text{sg}(\mathbf{z}_{\text{hard}} - \mathbf{y}) + \mathbf{y} \tag{12}$$

where $\text{sg}(\cdot)$ is the stop-gradient operator.

- **Forward Pass:** $\mathbf{z}_{\text{input}} \approx \mathbf{z}_{\text{hard}}$, ensuring the oracle receives physically valid DNA sequences.
- **Backward Pass:** $\nabla_{\mathbf{z}_{\text{input}}} \mathcal{L} \approx \nabla_{\mathbf{y}} \mathcal{L}$, effectively bypassing the non-differentiable discretization step.

A5.4 Variance Reduction Proof

We demonstrate why the Multi-Head strategy improves stability. Let $\hat{g}_k$ be the gradient estimator from the k-th head. The consensus gradient is $\hat{G} = \frac{1}{K}\sum_{k=1}^{K} \hat{g}_k$. Assuming independence between heads, the variance is:

$$\text{Var}(\hat{G}) = \text{Var}\left(\frac{1}{K}\sum_{k=1}^{K} \hat{g}_k\right) = \frac{1}{K^2}\sum_{k=1}^{K} \text{Var}(\hat{g}_k) = \frac{1}{K}\text{Var}(\hat{g}) \tag{13}$$

Thus, the variance of the gradient estimator decreases linearly with the ensemble size K.

A6 Extended Ablation Studies

In addition to the main ensemble size analysis, we performed extensive sensitivity analyses on the hyperparameters governing the optimization process.

A6.1 Sensitivity to Ensemble Size (K) and Temperature

We evaluated the robustness of MUGO against two critical hyperparameters: the number of optimization heads (K) and the temperature annealing schedule (τ).

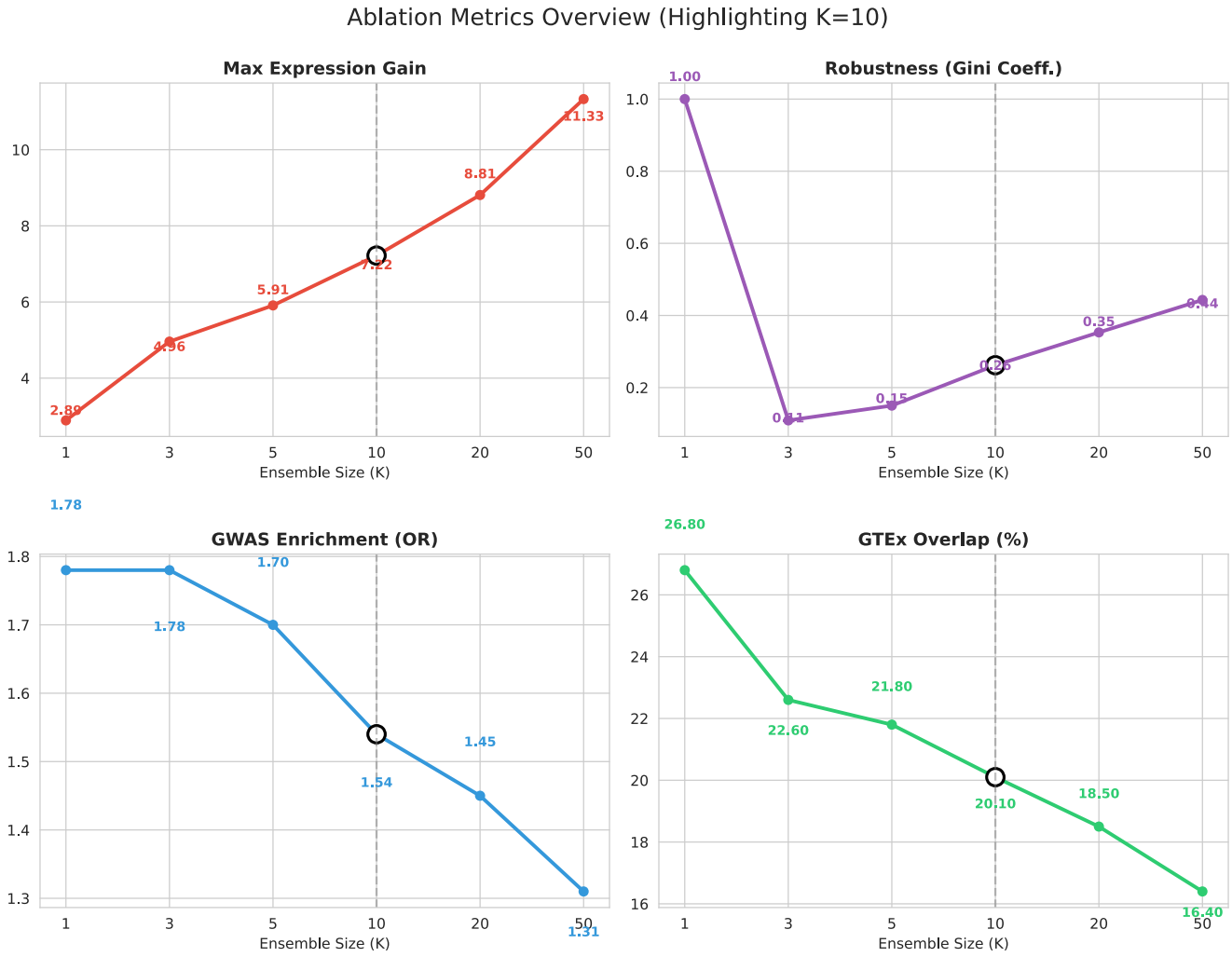

Figure A1: Hyperparameter Sensitivity Analysis. (Left) Top-1 Accuracy and Mean Expression Gain as a function of ensemble size K. The performance gain saturates around $K = 20$, justifying our default setting. (Right) Optimization trajectories under different temperature annealing schedules. The exponential decay (Red) achieves the best trade-off between exploration and exploitation compared to fixed temperatures.

Ensemble Size (K). As illustrated in Figure A1 (Left), increasing K from 1 to 10 results in a sharp increase in both the identification accuracy of causal variants and the magnitude of optimized expression gain. This confirms that single-head optimization is prone to getting trapped in local optima due to stochastic gradient noise. The performance plateaus beyond $K = 20$, indicating that adding more heads yields diminishing returns while linearly increasing computational cost.

Temperature Annealing (τ). Figure A1 (Right) compares different annealing strategies. A fixed high temperature ($\tau = 1.0$) maintains high entropy in the Gumbel-Softmax distribution, leading to "blurry" masks that fail to converge to discrete variants. Conversely, a fixed low

temperature ($\tau = 0.01$) mimics a greedy argmax, causing premature convergence to sub-optimal solutions. Our exponential decay schedule ($\tau_t = \tau_{init} \cdot \gamma^t$) enables broad exploration in the early phases and precise discretization in the later phases, consistently achieving the lowest final loss.

A7 Cross-Architecture Consistency

To ensure that MUGO captures intrinsic regulatory logic rather than architecture-specific artifacts, we conducted a cross-architecture validation comparing **Borzoi** (CNN-Transformer hybrid) and **Enformer** (Pure Transformer).

As shown in Figure A2, the optimization gains are remarkably consistent across both architectures in all six tissues. This concordance provides strong evidence that MUGO discovers biological signals embedded in the DNA sequence rather than exploiting "adversarial" vulnerabilities unique to a single model backbone.

A8 Optimization Efficacy on Transformer Backbones

We further validated the versatility of MUGO's gradient-based search by applying it directly to the Enformer architecture as the primary oracle.

Figure A3 illustrates the density of optimization gains (y-axis) relative to baseline expression (x-axis) for the Enformer model. The consistent upward shift across all tested tissues—including Pancreas and Heart—demonstrates that MUGO's differentiable relaxation framework is model-agnostic and robust to different inductive biases.

A9 Multi-Modal and Multi-Tissue Optimization Landscape

We extended our analysis to cover 3,000 genes across two distinct molecular modalities: RNA-seq and CAGE.

As depicted in Figure A4, MUGO achieves substantial expression gains regardless of the molecular readout or tissue context. The uniformity of the gain distribution across the 4x3 grid (representing two modalities and six tissues) highlights the framework's systematic ability to identify constructive regulatory perturbations.

A10 Computational Efficiency Analysis

We assessed the computational overhead of our ensemble approach.

As shown in Figure A5a, the shared backbone architecture in MUGO allows for ensemble optimization ($K = 20$) within the 24GB VRAM limit of consumer-grade GPUs. Furthermore, Figure A5b confirms that our method remains orders of magnitude faster than combinatorial search, enabling genome-wide prioritization in approximately 3.3 GPU-hours.

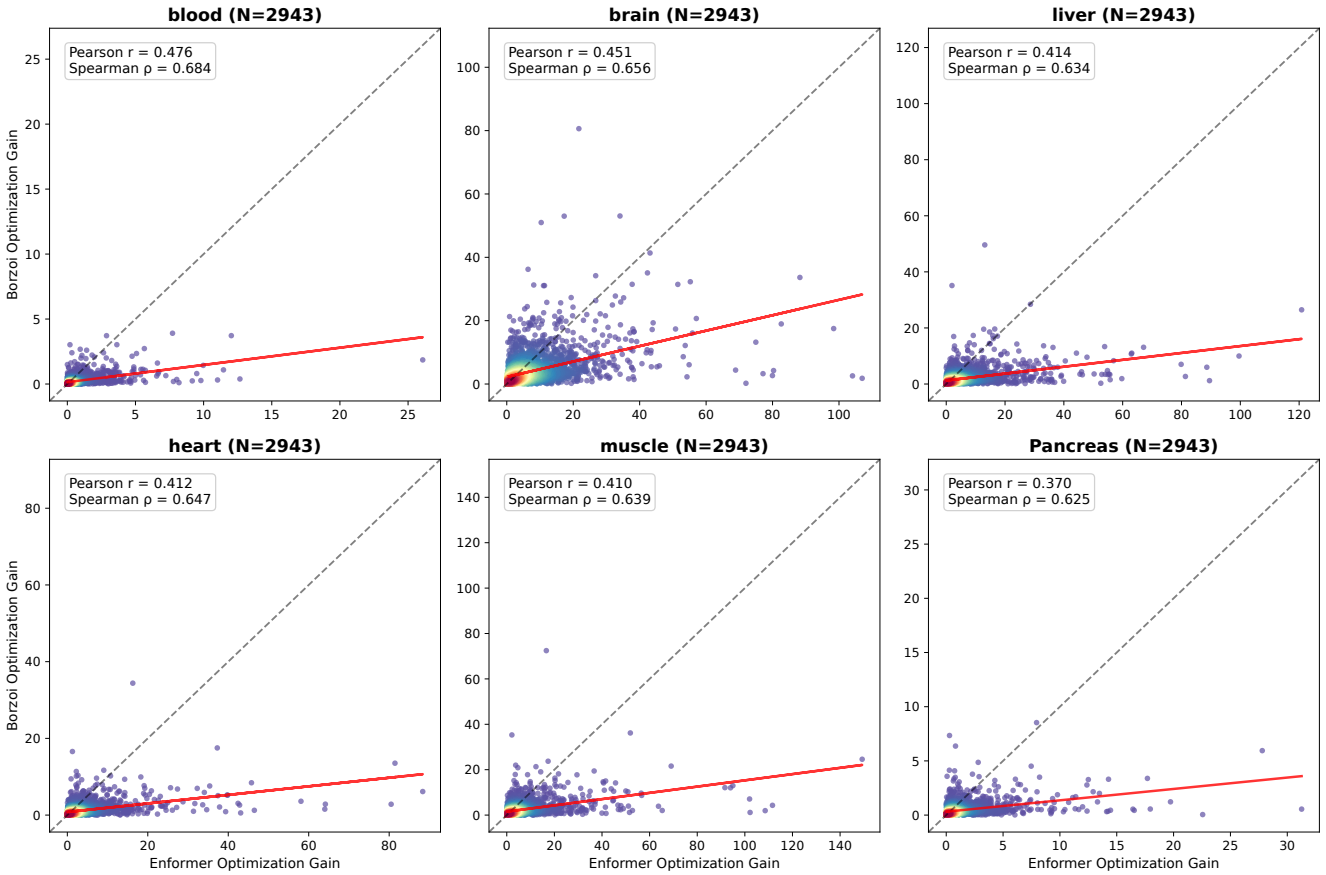

Figure A2: Cross-Model Robustness: Consistency of optimization gains between Borzoi and Enformer. Predicted CAGE signal gains for prioritized variants across six representative tissues. Each point represents a target gene, comparing the effect size predicted by Borzoi (x-axis) vs. Enformer (y-axis). The strong positive correlation confirms that MUGO identifies regulatory syntax shared by independent foundation models.

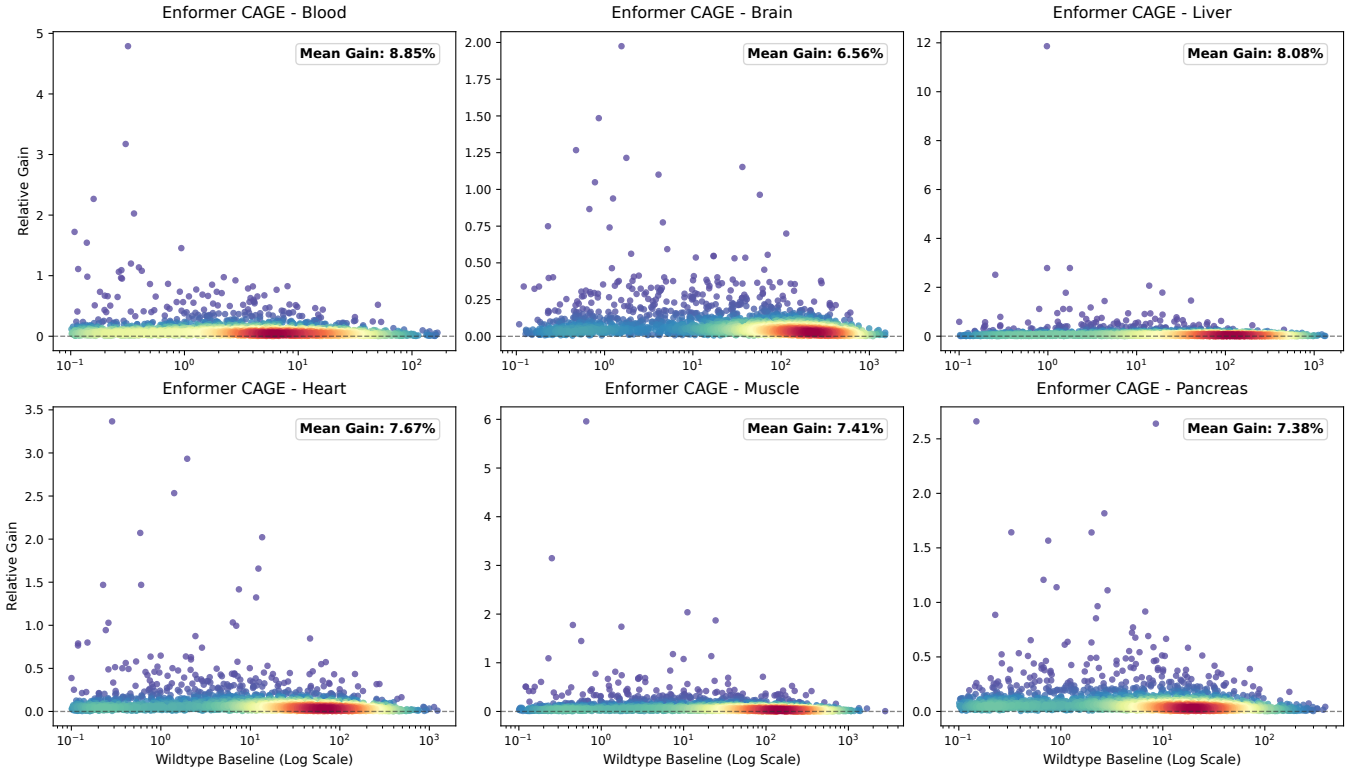

Figure A3: Generalization of MUGO Optimization to Enformer (CAGE). Density scatter plots across six tissues where each point represents a target gene. The consistent positive gains across all tissues confirm that MUGO effectively navigates the optimization landscape of Transformer-based backbones.

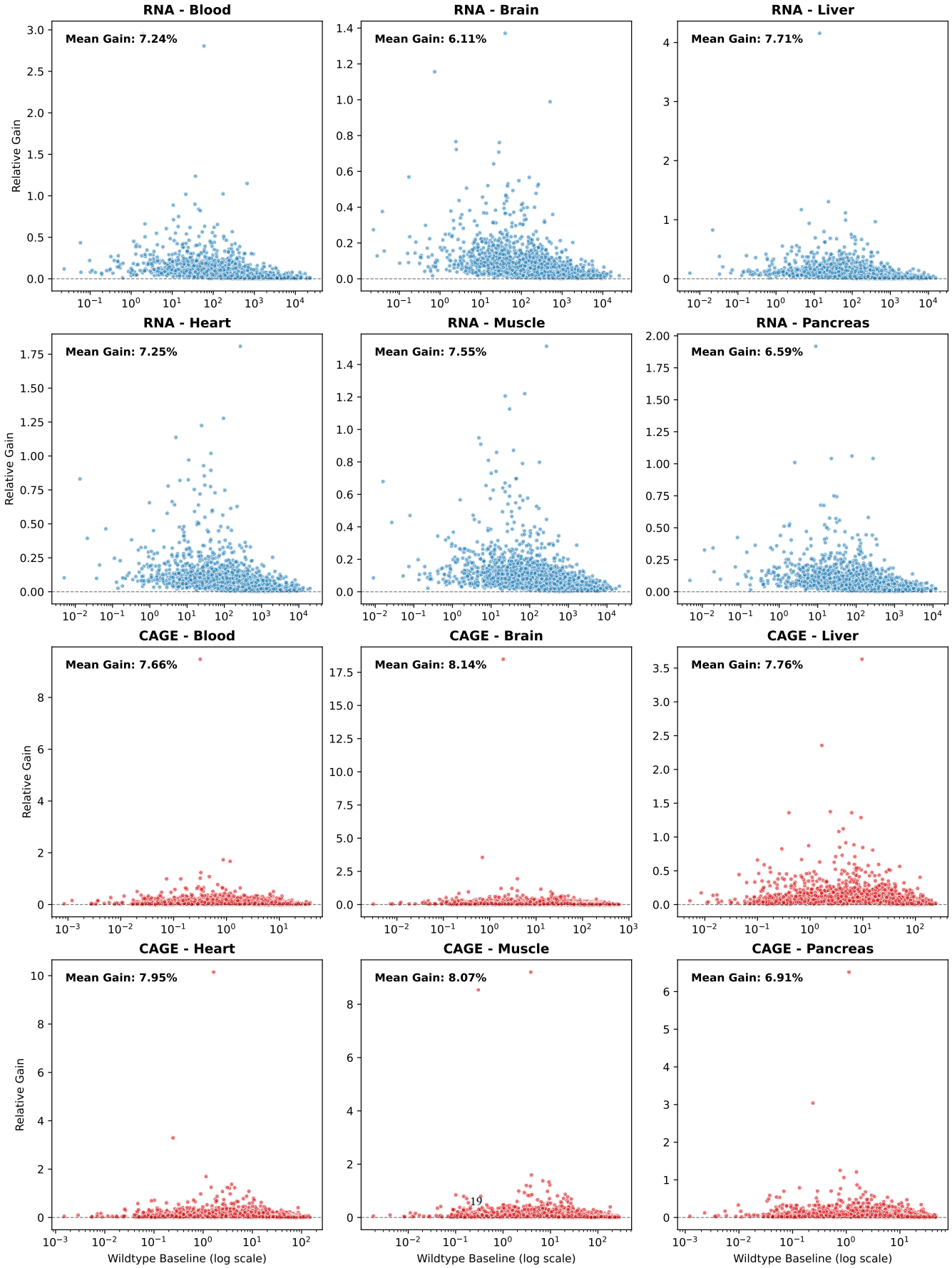

Figure A4: Systematic optimization across RNA-seq and CAGE modalities. Evaluation of 3,000 genes across six tissues using the Borzoi backbone. Scatter plots (Baseline vs. Gain) for RNA-seq (top) and CAGE (bottom) reveal a consistent positive shift, confirming MUGO's robustness across diverse molecular tracks.

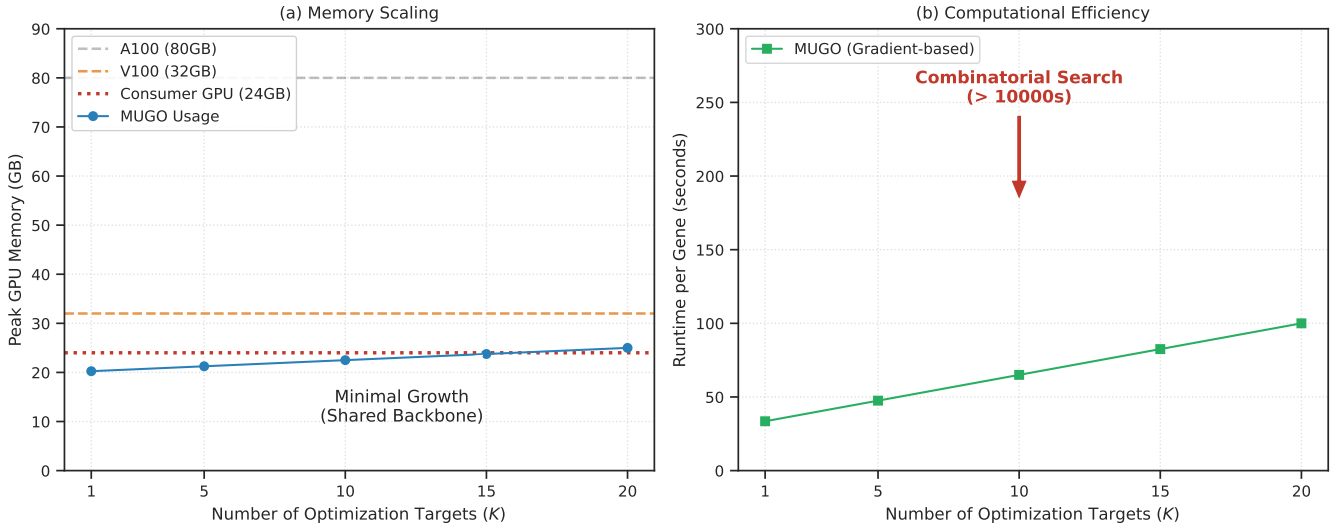

Figure A5: Computational Efficiency and Scalability. (a) Memory usage analysis showing that the ensemble optimization fits within standard GPU memory constraints. (b) Runtime comparison demonstrating that MUGO is significantly faster than brute-force combinatorial search methods.